

Disentangling New Physics in Single Resonant Top Quarks

Krish Wu*, Brandon Sun*, Nitish Polishetty*, Justin Kline*, Max Fieg, and Daniel Whiteson

Received May 19, 2025

Accepted October 12, 2025

Electronic access November 30, 2025

Collisions of particles at the energy frontier can reveal new particles and forces via localized excesses in invariant mass distributions. However, the initial observation may be consistent with a large variety of theoretical models, especially in sectors with new top quark partners, which feature a rich set of possible underlying interactions. We explore the power of the Large Hadron Collider dataset to distinguish between models of the singly produced heavy top-like quark which interacts with the Standard Model through an electromagnetic form factor. We study the heavy top decay to a top quark and a virtual photon which produces a pair of fermions, propose a technique to disentangle the models, and calculate the expected statistical significance to distinguish between various hypotheses.

Introduction

Many theories of new physics predict striking phenomena observable in high-energy collisions. In some cases, the potential experimental signatures are consistent with several distinct models of new particles or interactions, and disentangling them can be quite difficult^{1,2}. The discovery of the Higgs boson^{3,4}, for example, has been followed by precision measurements of its properties^{5,6} to determine whether it is the garden variety boson of the Standard Model, or something more exotic, a question whose answer is still being resolved. In the event that a discovery of a new particle is made, whether anticipated or not^{7,8}, it can be expected to spark a similar effort to distinguish potential theoretical explanations. The top quark sector has a rich set of models predicting new heavy partners, with multiple experimental signatures. In some cases, as in the scenario studied here, the nature of the production and decay can be quite similar across theoretical models, even if the form of the interactions is quite different.

Recently, we proposed⁹ the study of single production of a heavy vector-like quark T , which for high T masses features higher cross sections than pair production, and can include decays such as $T \rightarrow t\gamma$ ¹⁰, which can dominate in some scenarios¹¹ over the more commonly studied $T \rightarrow Wb, Zt, Ht$. Searches by the Large Hadron Collider (LHC) collaboration have primarily studied T decays featuring heavy bosons, $T \rightarrow Wb, Zt, Ht$ ¹²⁻²⁰. Studies of $T \rightarrow \gamma t$ have received less attention, and primarily focused on pair production of the new heavy fermion¹¹. ATLAS explored the $t\gamma$ final state²¹, but did not search for a $t\gamma$ resonance.

In this paper, we revisit single production of heavy vector-like quarks that interact through the photon via electromagnetic (EM) form factor operators. We study again the single produc-

tion mode and focus on the decay $T \rightarrow t\gamma \rightarrow tf^+f^-$, where the photon is off-shell and converts to a pair of fermions (f^+f^-). This mode is shared by the dimension-5 and dimension-6 EM form factor operators, which allows us to explore several distinct theoretical models, predict T production at the LHC, and examine the power of the LHC dataset to distinguish between these models.

The paper is organized as follows. The first section describes the theoretical models of the heavy top partner and the experimental sensitivity to the various models. The following sections discuss the results, and the final section describes the methods in detail.

Results

Models

Vector-like top partners²² are typically found in models that alleviate the hierarchy problem and are less constrained than a 4th generation of quarks with chiral couplings²³⁻²⁵. These particles can be found in more complete models such as Little Higgs models²⁶, supersymmetric theories, composite Higgs models²⁷ or in scenarios where the right-handed top quark is composite and T is an excited state^{28,29}. However, the compatibility of these motivations and the model we study are dependent on the details of the underlying theory.

In this work, we consider a class of models where a vector-like quark T , which has the same quantum numbers as a right-handed up-type quark, and can interact with the SM up-type quarks through electromagnetic form factor operators up to dimension-6. In particular, we consider an interaction taking the form of a dimension-5 magnetic and electric dipole moment (MDM, EDM), and the dimension-6 anapole and charge radius (CR) operators. The Lagrangians that govern these interactions

* These authors contributed equally to this work.

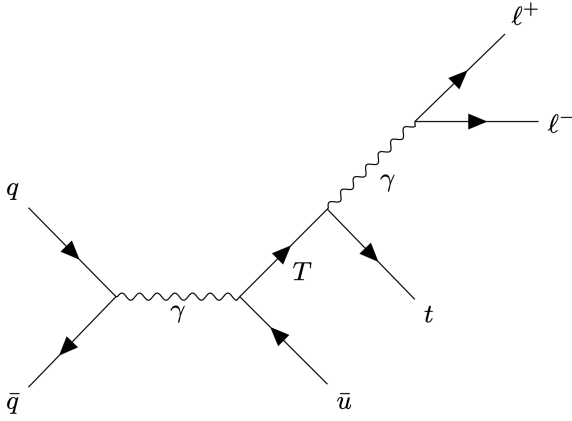


Fig. 1 Feynman diagram describing the single production of a heavy vector-like fermionic top partner T which decays to a top quark (t) and a photon (γ), which then decays to a pair of charged leptons ($\ell^+\ell^-$)

can be written as the following:

$$\mathcal{L}_{\text{MDM}} = \mu_i \bar{T} \sigma^{\mu\nu} u_{R,i} F_{\mu\nu}, \quad (1)$$

$$\mathcal{L}_{\text{EDM}} = d_i \bar{T} \sigma^{\mu\nu} \gamma^5 u_{R,i} F_{\mu\nu}, \quad (2)$$

$$\mathcal{L}_{\text{Anapole}} = a_i \bar{T} \gamma^\mu \gamma^5 u_{R,i} \partial^\nu F_{\mu\nu}, \quad (3)$$

$$\mathcal{L}_{\text{CR}} = b_i \bar{T} \gamma^\mu u_{R,i} \partial^\nu F_{\mu\nu} \quad (4)$$

where $u_{R,i}$ is a right-handed up-type quark, μ_i, d_i, a_i, b_i are dimensionful couplings of T to a quark with flavor i . This effective interaction can arise in a UV model where heavy particles with electroweak charges have been integrated out¹¹ or where the top quark is composite, and these interactions mediate radiative transitions with the excited state T ³⁰. The dimension-6 operators are studied less frequently in the literature, but we nevertheless wish to assess their signatures as they could generically arise through analogous mechanisms. The physics responsible for these interactions is at or above the TeV-scale. For $m_T \approx \text{O}(\text{TeV})$, the new state can only be directly produced at the LHC, and may be searched for with jet + photon signatures³¹ for the EDM and MDM operators, while the higher dimensional operators could be searched for with trijet signatures³² or dilepton + jet. Some of these interactions can also be searched for indirectly, in particular the anapole and EDM operators lead to parity violation which can be indirectly tested in atomic systems³³. The dimension-5 operators induce a $T \rightarrow t\gamma$ decay, and while the partial decay width of this channel for the dimension-6 operators is zero for an on-shell photon, the offshell photon decaying to a pair of fermions has nonzero width. Thus, the four models produce tf^+f^- , allowing a direct comparison of the kinematics in the same final states.

Table 1 Expected yields (N) in 300 fb^{-1} of LHC pp collisions at $\sqrt{s} = 13 \text{ TeV}$ for several background processes. Cross sections for backgrounds are at NLO in QCD³⁴.

Process	N
$t\bar{t}\gamma$	2730
$Z + b\bar{b} + \gamma$	681
$W + b\bar{b} + \gamma$	256
$i\bar{b}\gamma + i\bar{t}b\gamma$	21

Experimental Sensitivity

The models described above include interactions which can generate a final state with a top quark and a pair of opposite-sign charged leptons; see Figure 1. We estimate the sensitivity of the LHC dataset to these hypothetical signals using samples of simulated pp collisions at $\sqrt{s} = 13 \text{ TeV}$ with an integrated luminosity of 300 fb^{-1} . Generation of simulated signal and background events as well as the reconstruction strategy are described below.

The dominant backgrounds are the production of topquark pairs with an additional pair of leptons ($t\bar{t}\ell^+\ell^-$), or the production of a single top quark in association with a b quark ($t\bar{b}\ell^+\ell^-$) and a pair of leptons. Additional backgrounds are due to production of a heavy vector boson (W or Z bosons) in association with b quarks and a pair of leptons, $Wb\bar{b}\ell^+\ell^-$ or $Zb\bar{b}\ell^+\ell^-$. Contribution from QCD multi-jet production is suppressed by the lepton requirement and the minimum m_T , and are non-zero but sub-dominant and are neglected here. Distributions of the expected reconstructed T quark masses and the photon transverse momentum for the background and signal processes are shown in Figure 3 and the expected background yields in 300 fb^{-1} are shown in Table 1.

Statistical Analysis

Expected limits on the single T production cross section are calculated at 95% confidence level (CL) using a profile likelihood ratio³⁵ with the CLs technique^{36,37}. We use the pyhf^{38,39} package with a binned distribution in heavy quark reconstructed mass, where bins without simulated background events have been merged into adjacent bins. The background is assumed to have a 50% relative systematic uncertainty. Limits on the signal cross section as a function of the T quark mass are shown in Figure 4.

Distinguishing between the various models using only the reconstructed heavy quark invariant mass would be challenging given the similarity in the mass distributions. But there is more information present in the events that can reveal the nature of the underlying interaction. The dimension-6 operators have an additional dependence on the virtual photons momenta in the Lagrangian, as shown in equations 1-4, and thus will display a strong difference in the kinematic distribution in the final state

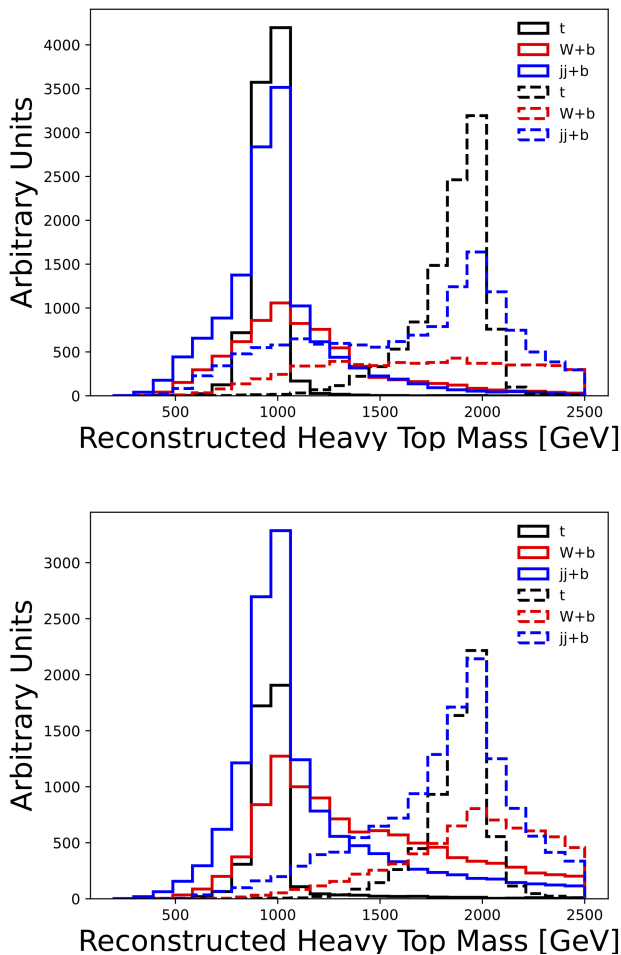


Fig. 2 Distribution of the reconstructed heavy top (T) quark candidate mass in simulated events with $m_T = 1000$ (solid) or 2000 (dashed) GeV, for MDM (top) and Anapole (bottom) models for each of the three reconstruction strategies (see Fig 7). The overall normalization is arbitrary, but the relative density of reconstruction modes reflects the different top quark p_T predicted by the two models in the $T \rightarrow t\gamma$ decay.

leptons, as is seen in the distribution of reconstructed photon momentum in the bottom panel of Figure 3. Distributions for MDM and EDM models are very similar, as those from the CR and Anapole models; only CR and EDM are shown, for two choices of m_T .

To capture the full discrimination information available, we train a neural network (NN) to distinguish between the heavy quark models. The network inputs are the four vectors of the reconstructed top quark and photon. Three hidden layers are used, consisting of 100 nodes, 80 nodes, and 20 nodes respectively, each with a ReLU activation. The final layer has a single sigmoid neuron. In training, the dimension-5 models were given

label 0 and the dimension-6 models label of 1. The loss function is binary cross entropy and mini-batch training with batch sizes of 10 was used, along with the Adam optimizer. Each sample had approximately 100,000 events, and an independent network was trained for each of the candidate heavy quark masses considered. One quarter of the data were reserved for testing, and training continued until performance plateaued on the testing sample, to avoid overfitting.

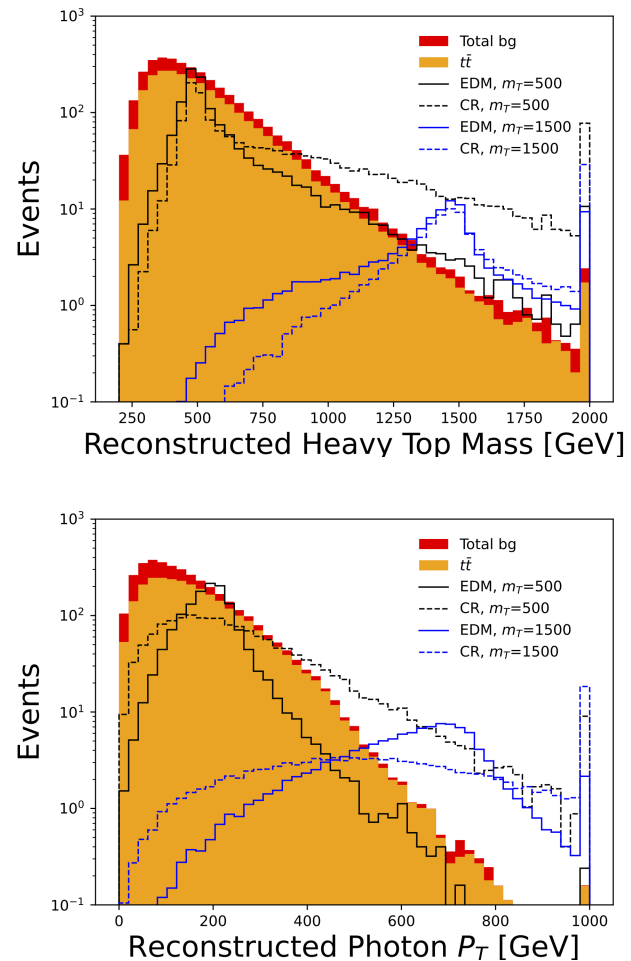


Fig. 3 Distribution of reconstructed heavy quark invariant mass (top) or photon p_T in simulated signal and background samples, normalized to an integrated luminosity of 300 fb^{-1} . The last bin shows overflow. The signal cross section is set to the expected limit at 95% CL.

The output of the network and its discrimination power is shown in Figure 5, showing significantly more discrimination power than the top or photon transverse momenta individually.

To assess the power of the dataset to distinguish between these models, we calculate the likelihood ratio (LR) between the dimension-5 and dimension-6 models using the binned network output to estimate the densities. We calculate the p-value under

the dimension-5 scenario of observing the mean LR expected in the dimension-6 scenario as a function of the signal cross section, and vice versa. Results are shown in Figure 6 and indicate that as the heavy quark mass increases, the signal cross section needed to obtain a p-value of less than 0.05 decreases, due to falling background rates. For $m_T \approx 1000$ GeV, sufficient statistics can be achieved for 300 fb^{-1} , for a cross section greater than about 0.1 fb .

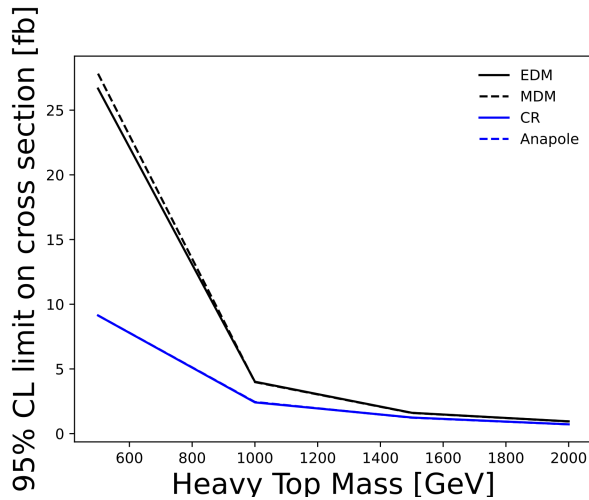


Fig. 4 Expected 95% CL upper limits on the production cross section for signal models, as a function of heavy top quark mass.

Discussion

While the various models produce the same list of final state objects and very similar heavy quark mass distributions, the full kinematics of the events allow us to disentangle the dimension-5 and dimension-6 hypotheses. There are additional handles that might help, such as searching for on-shell production of photons, which are expected in dimension-5 models but not in dimension-6. The on-shell photon in dimension-5 models also allow for a photon in the initial state, where $\gamma q \rightarrow T \rightarrow t\gamma$ gives a very similar final state and could contribute to the production rate, though the photon parton distribution function (PDF) is more uncertain than quark PDFs. Other experiments and final states can also play an important role. In the event of non-zero mixing between T and u_R , electroweak precision observables can be used to constrain mixing parameters^{40–43}. Furthermore, flavor changing neutral current processes have been used to constrain vector-like fermions^{44–48}. In addition to direct searches at the LHC, vector-like quarks in the $O(100)$ GeV mass range can be searched for at the Tevatron⁴⁹. The studies above demonstrate the possibility of distinguishing between dimension-5 and dimension-6 electromagnetic form factor models, but do not explore whether data could be used to prefer one of the mod-

els of equal dimensionality. The kinematics of the production and decay appear to be indistinguishable upon inspection of the distributions and attempts to train a machine learning model.

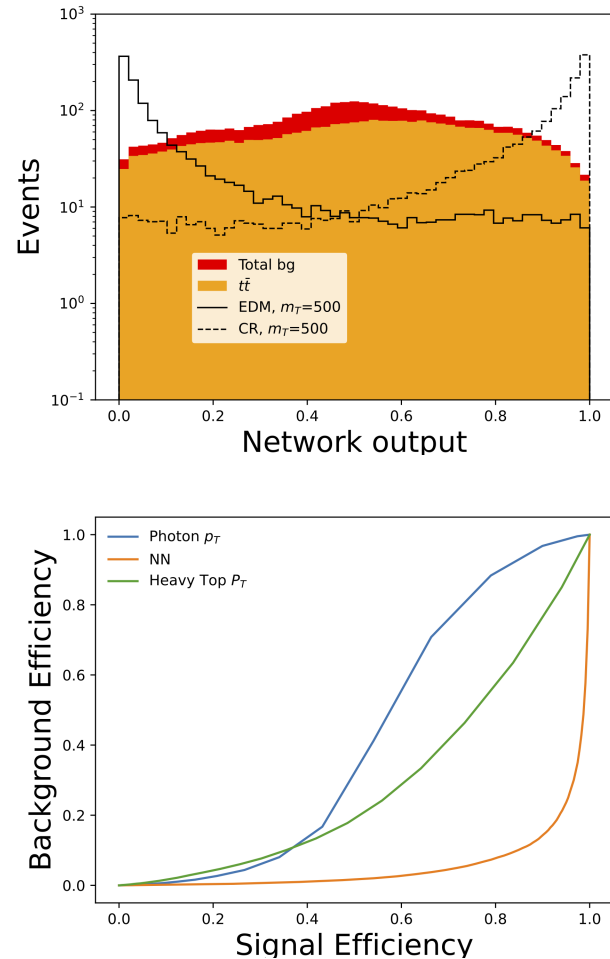


Fig. 5 Top: distribution of neural network output trained for the $m_T = 500$ GeV scenario, shown for simulated signal and background samples normalized to an integrated luminosity of 300 fb^{-1} . The signal cross section is set to the expected limit at 95% CL. Bottom: Signal and background efficiency for various thresholds on photon transverse momentum, heavy quark transverse momentum or the neural network output, also for the $m_T = 500$ GeV case.

While our methods do not distinguish between operators of the same dimension, it may be possible to differentiate these models by leveraging observables related to angular correlations of the final state particles, which are sensitive to the CP structure of the interaction^{50,51}. Theoretically, distinguishing between parity-conserving and parity-violating operators of the same dimension could be achieved using a polarized beam, an option not available at the LHC, but potentially feasible at a future electron⁵² or muon collider⁵³. While these models do

predict differences in the overall production rate at the LHC, the unknown coupling strength means that an observed rate could be compatible with either scenario.

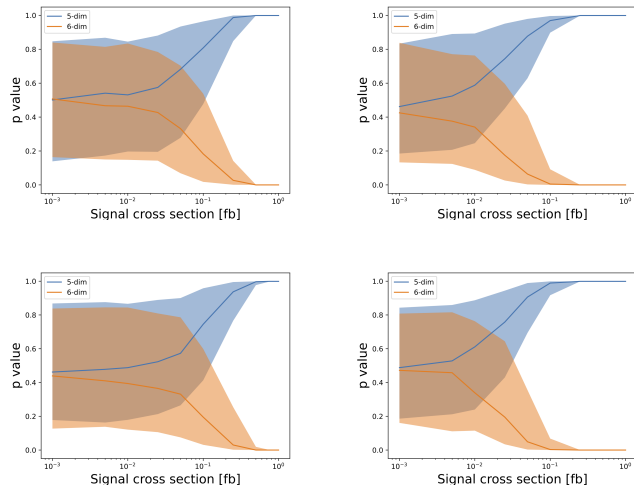


Fig. 6 Expected p -values under a dimension-5 hypothesis of observing a neural network output distribution expected from the dimension-6 hypothesis, and vice versa, as a function of the signal production cross section. Shown are the median case (solid line) and an envelope containing 95% of hypothetical similar experiments for the 500, 1000, 1500 and 2000 GeV scenarios (top to bottom).

In conclusion, we present an example of a set of theoretical models which have different underlying mechanisms but would produce similar excesses in reconstructed invariant mass peaks. The theoretical distinctions lead to differences in other kinematic information in the event, which can be exploited in this case to disentangle two categories of models, those with dimension-5 and dimension-6 operators. We train a neural network to capture and summarize these differences. In a pp collision dataset at $\sqrt{s} = 13$ TeV with 300 fb^{-1} and $m_T \approx 1000$ GeV, signal cross sections of approximately 0.1 fb are required to provide sufficient statistics to distinguish between the various hypotheses at 95% CL.

Methods

Samples of simulated signal and background events are used to model the reconstruction of the T quark candidates, estimate selection efficiencies and expected signal and background yields. Collisions and decays are simulated with Madgraph5 v3.5.7⁵⁴ with nnpdf v2.3⁵⁵ and renormalization and factorization scales set to m_Z , and Pythia v8.306⁵⁶ is used for fragmentation and hadronization. Radiation of additional gluons is modeled by Pythia. The detector response is simulated with Delphes v3.5.0⁵⁷ using the standard CMS card, extended to include an additional reconstruction of wide cone jets, and root

version 5.34.25⁵⁸.

Selected isolated photons and leptons are required to have transverse momentum $p_T \geq 10$ GeV and absolute pseudo-rapidity $0 \leq |\eta| \leq 2.5$. Isolation requires that less than 12% (25%) of the p_T of the electron or photon (muon) be deposited in a cone with $\Delta R < 0.5$ centered on the particle. Selected narrow-cone (wide-cone) jets are clustered using the anti-kT algorithm⁵⁹ with radius parameter $R = 0.4$ ($R = 1.2$) using FastJet 3.1.2⁶⁰ and are required to have $p_T \geq 20$ GeV and $0 \leq |\eta| \leq 2.5$. Wide-cone jets with mass within $[50, 110]$ ($[125, 225]$) GeV are tagged as W-boson (top-quark) jets. Events are required to have exactly two opposite-sign electrons or muons, which are combined to reconstruct the photon candidate.

Reconstruction of the top quark can proceed in several ways due to the various decay modes of the W boson. The hadronic decay mode is typically the most powerful^{61,62} due to its high branching fraction and techniques to efficiently reconstruct its decay using large radius jets and state-of-the-art tagging algorithms. The background from multijet events can be accurately modeled using data driven methods. Candidate T quarks are reconstructed from the combination of the off-shell photon candidate (via the observed lepton pair) and the top quark candidate, which is reconstructed in one of three approaches:

- t : one top-tagged, b -tagged wide-cone jet
- $W + b$: one W -tagged, un- b -tagged wide-cone jet and one b -tagged narrow-cone jet
- $jj + b$: two un- b -tagged narrow-cone jets and one b -tagged narrow-cone jet

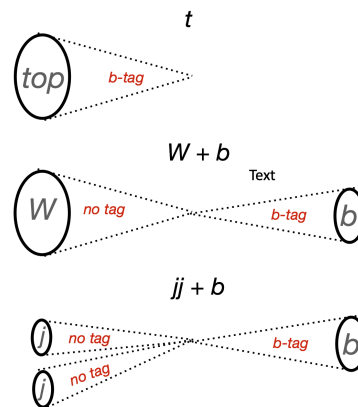


Fig. 7 Three possible top quark reconstruction strategies, using wide-cone and narrow-cone jets, which can be b -tagged, W -tagged or top-tagged. See text for details.

The three approaches are illustrated in Figure 7. If several reconstruction approaches are available for a single event, preference is given to t and then $W + b$. If several jets are available

within one approach, preference is given to the jets that minimize the difference between the reconstructed and known top-quark and W -boson masses. Events with no T quark candidate with mass greater than 200 GeV are rejected. Distributions of reconstructed T quark candidate masses are shown in Figure 2 for two representative models.

Acknowledgment

DW was funded by the DOE Office of Science. The work of M.Fieg was supported by NSF Grant PHY2210283 and was also supported by NSF Graduate Research Fellowship Award No. DGE-1839285. The authors thank Tim Tait, Avik Roy, Jeong Han Kim and KC Kong for useful comments.

References

- 1 N. Arkani-Hamed, G. L. Kane, J. Thaler and L.-T. Wang, *JHEP*, 2006, **08**, 070.
- 2 J. Alwall, P. Schuster and N. Toro, *Phys. Rev. D*, 2009, **79**, 075020.
- 3 G. Aad *et al.*, *Phys. Lett. B*, 2012, **716**, 1–29.
- 4 S. Chatrchyan *et al.*, *Phys. Lett. B*, 2012, **716**, 30–61.
- 5 G. Aad *et al.*, *JHEP*, 2023, **07**, 088.
- 6 A. M. Sirunyan *et al.*, *JHEP*, 2021, **07**, 027.
- 7 N. Craig, P. Draper, K. Kong, Y. Ng and D. Whiteson, *Acta Phys. Polon. B*, 2019, **50**, 837.
- 8 J. H. Kim, K. Kong, B. Nachman and D. Whiteson, *JHEP*, 2020, **04**, 030.
- 9 S. Tong, J. Corcoran, M. Fieg, M. Fenton and D. Whiteson, *JHEP*, 2024, **02**, 057.
- 10 J. H. Kim and I. M. Lewis, *JHEP*, 2018, **05**, 095.
- 11 H. Alhazmi, J. H. Kim, K. Kong and I. M. Lewis, *JHEP*, 2019, **01**, 139.
- 12 M. Aaboud *et al.*, *Phys. Rev. Lett.*, 2018, **121**, 211801.
- 13 M. Aaboud *et al.*, *JHEP*, 2017, **10**, 141.
- 14 A. Tumasyan *et al.*, *JHEP*, 2023, **09**, 057.
- 15 A. Tumasyan *et al.*, *JHEP*, 2022, **05**, 093.
- 16 A. M. Sirunyan *et al.*, *Phys. Rev. D*, 2020, **102**, 112004.
- 17 A. Roy, N. Nikiforou, N. Castro and T. Andeen, *Phys. Rev. D*, 2020, **101**, 115027.
- 18 G. Aad *et al.*, *Phys. Rev. D*, 2022, **105**, 092012.
- 19 G. Aad *et al.*, *JHEP*, 2023, **08**, 153.
- 20 G. Aad *et al.*, *Eur. Phys. J. C*, 2023, **83**, 719.
- 21 G. Aad *et al.*, *Phys. Rev. Lett.*, 2023, **131**, 181901.
- 22 J. a. M. Alves, G. C. Branco, A. L. Cherchiglia, C. C. Nishi, J. T. Penedo, P. M. F. Pereira, M. N. Rebelo and J. I. Silva-Marcos, 2023.
- 23 J. A. Aguilar-Saavedra, R. Benbrik, S. Heinemeyer and M. Pérez-Victoria, *Physical Review D*, 2013, **88**, 094010.
- 24 B. A. Dobrescu and C. T. Hill, *Phys. Rev. Lett.*, 1998, **81**, 2634–2637.
- 25 K. du Plessis, M. M. Flores, D. Kar, S. Sinha and H. van der Schyf, *SciPost Phys.*, 2022, **13**, 018.
- 26 M. Schmaltz and D. Tucker-Smith, *Ann. Rev. Nucl. Part. Sci.*, 2005, **55**, 229–270.
- 27 O. Witzel, *PoS*, 2019, **LATTICE2018**, 006.
- 28 B. Lillie, J. Shu and T. M. P. Tait, *JHEP*, 2008, **04**, 087.
- 29 A. Delgado and T. M. P. Tait, *JHEP*, 2005, **07**, 023.
- 30 A. Belyaev, R. S. Chivukula, B. Fuks, E. H. Simmons and X. Wang, *Phys. Rev. D*, 2023, **108**, 035016.
- 31 M. Aaboud *et al.*, *Eur. Phys. J. C*, 2018, **78**, 102.
- 32 A. M. Sirunyan *et al.*, *Phys. Lett. B*, 2020, **805**, 135448.
- 33 B. K. Sahoo, B. P. Das and H. Spiesberger, *Phys. Rev. D*, 2021, **103**, L111303.
- 34 J. Alwall, R. Frederix, S. Frixione, V. Hirschi, F. Maltoni, O. Mattelaer, H. S. Shao, T. Stelzer, P. Torrielli and M. Zaro, *JHEP*, 2014, **07**, 079.
- 35 G. Cowan, K. Cranmer, E. Gross and O. Vitells, *Eur. Phys. J. C*, 2011, **71**, 1554.
- 36 T. Junk, *Nucl. Instrum. Meth. A*, 1999, **434**, 435–443.
- 37 A. L. Read, *J. Phys. G*, 2002, **28**, 2693–2704.
- 38 L. Heinrich, M. Feickert and G. Stark, *pyhf: v0.7.3*, <https://doi.org/10.5281/zenodo.1169739>, <https://github.com/scikit-hep/pyhf/releases/tag/v0.7.3>.
- 39 L. Heinrich, M. Feickert, G. Stark and K. Cranmer, *Journal of Open Source Software*, 2021, **6**, 2823.
- 40 C.-Y. Chen, S. Dawson and I. M. Lewis, *Physical Review D*, 2014, **90**, 035016.
- 41 C.-Y. Chen, S. Dawson and E. Furlan, *Physical Review D*, 2017, **96**, 015006.
- 42 S. Dawson and E. Furlan, *Physical Review D*, 2012, **86**, 015021.
- 43 D. Choudhury, T. M. P. Tait and C. E. M. Wagner, *Phys. Rev. D*, 2002, **65**, 053002.
- 44 K. Ishiwata, Z. Ligeti and M. B. Wise, *Journal of High Energy Physics*, 2015, **2015**, 027.
- 45 A. Collaboration, *Physical Review D*, 2018, **98**, 032002.
- 46 F. del Aguila and J. Corts, *Physics Letters B*, 1985, **156**, 243–249.
- 47 Z. Kang and Y. Shigekami, *Journal of High Energy Physics*, 2019, **2019**, 049.
- 48 S. Balaji, *JHEP*, 2022, **05**, 015.
- 49 Y. Okada and L. Panizzi, *Adv. High Energy Phys.*, 2013, **2013**, 364936.
- 50 D. Gonçalves, K. Kong and J. H. Kim, *JHEP*, 2018, **06**, 079.
- 51 D. Gonçalves, J. H. Kim, K. Kong and Y. Wu, *JHEP*, 2022, **01**, 158.

-
- 52 A. Blondel *et al.*, 2019.
- 53 B. Norum and R. Rossmanith, *Nucl. Phys. B Proc. Suppl.*, 1996, **51**, 191–200.
- 54 J. Alwall, R. Frederix, S. Frixione, V. Hirschi, F. Maltoni *et al.*, *JHEP*, 2014, **1407**, 079.
- 55 R. D. Ball *et al.*, *Eur. Phys. J. C*, 2021, **81**, 958.
- 56 T. Sjostrand, S. Mrenna and P. Z. Skands, *JHEP*, 2006, **0605**, 026.
- 57 J. de Favereau *et al.*, *JHEP*, 2014, **1402**, 057.
- 58 R. Brun and F. Rademakers, *Nucl. Instrum. Meth. A*, 1997, **389**, 81–86.
- 59 M. Cacciari, G. P. Salam and G. Soyez, *JHEP*, 2008, **04**, 063.
- 60 M. Cacciari, G. P. Salam and G. Soyez, *Eur.Phys.J.*, 2012, **C72**, 1896.
- 61 A. M. Sirunyan *et al.*, *JHEP*, 2019, **04**, 031.
- 62 G. Aad *et al.*, *JHEP*, 2020, **10**, 061.